The Astrophysical Journal, 948:70 (8pp), 2023 May 1 https://doi.org/10.3847/1538-4357/acc52b

Episodes of Molecular Emission in the Optical Spectrum of IRAS 22272+5435

Kārlis Puķītis[1], Laimons Začs[1], and Julius Sperauskas[2]
[1] Laser Center, Faculty of Physics, Mathematics, and Optometry, University of Latvia, Raia bulvāris 19, LV-1586 Rīga, Latvia; karlis.pukitis@lu.lv
[2] Vilnius University Observatory, Saulėtekio al. 3, 10257 Vilnius, Lithuania
Received 2023 January 25; revised 2023 March 15; accepted 2023 March 15; published 2023 May 8

Abstract

Emission of carbon-bearing molecular lines in multiple optical spectra of IRAS 22272+5435 from 2015 to 2017 is detected, and, for the first time in post–asymptotic giant branch stars, real-time evolution of these features is observed. Specifically, lines of various vibrational transitions of the CN Red system and C_2 Swan system are identified to be in emission. Contrary to the narrow and blueshifted AGB ejecta absorption lines, the emission profiles are broad and redshifted or blueshifted by no more than a few kilometers per second. Molecular emissions appear to be exclusive to spectra corresponding to pulsation phases closer to the star's light maxima than minima, but there are also such spectra without emissions. The time required for emissions to reach the largest observed intensity or decrease to absorption is around 2–3 weeks. The C_2 Phillips system lines are observed to have emission components as well, but no evidence for their short-term variability is found. It is proposed that the observed emissions originate within few stellar radii above the photosphere.

Unified Astronomy Thesaurus concepts: Post-asymptotic giant branch stars (2121); Stellar atmospheres (1584); High resolution spectroscopy (2096); Circumstellar gas (238); Stellar winds (1636); Shocks (2086)

1. Introduction

Due to their rapid evolution, post–asymptotic giant branch (post-AGB) objects—one of the late evolution stages of low- and intermediate-mass stars—are not found in large numbers. This is one of the reasons that leads to them being among the least understood phases of stellar evolution. Another often contributing factor, apart from some post-AGB stars being heavily obscured by a nebula of gas and dust created during the precursory AGB stage, is the wide range of peculiarities in their optical spectra (see, for example, Lèbre et al. 1996; Sánchez Contreras et al. 2008; Klochkova 2014; Bollen et al. 2022). One such anomaly is emission in optical molecular lines. The C_2 Swan system emissions have been observed in IRAS 04296+3429 (Klochkova et al. 1999; Sánchez Contreras et al. 2008), IRAS 23304+6147 (Klochkova et al. 2000a), IRAS 22223+4327 (Klochkova et al. 2010), and RAFGL 2688 (Klochkova et al. 2000b), for which C_2 Phillips system emissions have also been detected (Bakker et al. 1997). The CH^+, CH, and CN emissions have been found in the spectrum of RAFGL 915 (Hobbs et al. 2004). Also, emissions associated with diffuse interstellar bands have been observed in this object (Schmidt et al. 1980; Sarre et al. 1995). The site of formation of molecular emissions is not always clear. For example, according to Sánchez Contreras et al. (2008), C_2 features in IRAS 04296+3429 originate not in the extended nebula but in a compact region closer to the central star. On the contrary, Klochkova et al. (2000a) suggested that it is exactly the contribution of the matter further from the star that causes emissions to be seen in the spectrum.

Object IRAS 22272+5435 is a well-known, bright, G-type post-AGB star that pulsates in a complex fashion with a dominant period of 132 days (Hrivnak et al. 2013). According to Ueta et al. (2001), the nebula surrounding the star consists of three main components, with the outer and most extensive one being the AGB shell, the result of mass loss during the previous evolutionary stage. Then follows the superwind shell, located at around $1–5 \times 10^{16}$ cm from the central star (adjusted for the Gaia DR3 distance of 1.41 kpc; Oudmaijer et al. 2022). This component is of a near-toroidal shape, and it was created by intense axisymmetric wind at the very end of the AGB phase. The innermost part—the post-AGB shell—consists of material that the star has expelled during the current evolutionary phase.

Apart from an extreme variation in the intensity of optical molecular absorptions that follows stellar pulsation and splitting of strong metallic absorption lines, another abnormality in the spectrum of this star is the weak CN Red system (5, 1) emissions that appear during light and surface temperature maximum phases (Začs et al. 2009, 2016) and P Cygni–like profiles of C_2 Phillips (1, 0) lines (Schmidt et al. 2013). Variation of molecular emission features in IRAS 22272+5435 has also been observed in the *K* band. Hrivnak et al. (1994) detected emission of CO $\Delta v = 2$ bands, and after approximately 3 months, these features were seen in absorption. Venkata Raman & Anandarao (2008) observed the same CO bands in absorption, and after 1.5 months, these features were absent.

This study continues the research of short-term variability in the optical spectra of IRAS 22272+5435 (Začs & Puķītis 2021), as we report here emission of carbon-bearing molecular features and their evolution on a timescale as short as 1 week.

2. Observations

We have observed the spectra of IRAS 22272+5435 on 23 different nights during the time span from 2015 October until 2017 October with VUES (Jurgenson et al. 2016), mounted on the 1.65 m telescope at Moletai Astronomical Observatory. Here we present an analysis of spectra from three epochs on 2015 September 30–October 15 and four spectra from 2015 December 7–2016 January 5. Additionally, we use a spectrum

Table 1
The Analyzed Spectra of IRAS 22272+5435 from 2015 September to 2016 January

Spectrograph	Date	MJD	S/N	V_r (km s^{-1})	Phase
ESPaDOnS	2015/9/22	57,287.3	410	−41.8	0.62
VUES	2015/9/30	57,296.0	150	−40.9	0.69
VUES	2015/10/6	57,301.9	235	−40.7	0.73
VUES	2015/10/7	57,303.0		−40.7	0.74
VUES	2015/10/14	57,310.0	170	−40.7	0.80
VUES	2015/10/15	57,310.8		−40.9	0.80
VUES	2015/12/7	57,363.9	75	−37.7	0.20
VUES	2015/12/16	57,372.8	120	−38.7	0.27
VUES	2015/12/28	57,384.8	90	−41.2	0.36
VUES	2016/1/5	57,392.8	80	−42.5	0.42

Note. The S/N ratio is shown for the summed 6 and 7 and 14 and 15 spectra; see Section 3.1.

observed with ESPaDOnS[3] at CFHT on 2015 September 22, which we extracted from the CFHT Science Archive. Also, a spectrum of HD 21699 observed with ESPaDOnS on the same night as IRAS 22272+5435 was retrieved from the archive for identification of telluric absorption lines. Specific dates, average signal-to-noise ratios (S/Ns), heliocentric radial velocities, and estimated pulsation phases are show in Table 1.

Radial velocities are measured using around 160 weak and medium-strength absorption lines in each spectrum by cross-correlating the profiles with their mirror profiles. We utilize some of the least blended lines that were used for precise photospheric parameter estimation and abundance analysis by Začs & Puķītis (2023). For all of the spectra, the statistical error for radial velocity is no larger than 0.3 km s^{-1}. The radial velocity zero-point is controlled by observations of the IAU radial velocity standards and by inspecting the positions of the telluric absorption lines. We estimate that the systematic radial velocity offset is no larger than 0.1 km s^{-1}. The widths of the telluric lines suggest a spectral resolution of $R = \lambda/\Delta\lambda \sim 54{,}000$ and 29,000 for ESPaDOnS and VUES spectra. The VUES spectra continuously cover wavelengths ranging from 4060 to 9096 Å. The ESPaDOnS spectrum reaches from 3694 to 10482 Å with between-order gaps from 9224 to 9233 Å, from 9608 to 9634 Å, and from 10026 to 10072 Å.

The VUES spectra were reduced using the automated pipeline described in Jurgenson et al. (2016), and the ESPaDOnS spectra from the CFHT Science Archive were retrieved having been already reduced using the Libre-ESpRIT package (Donati et al. 1997). The latter consist of multiple exposures at different polarizations; however, no significant differences were found between them, so the summed (intensity) spectrum was used. Multiple VUES exposures that were acquired during a single night were summed to increase the S/N in the case of the September 30–October 15 data. For all of the spectra, the continuum was normalized by dividing them with a spline fitted to interactively placed continuum points. Continuum normalization and measurement of radial velocities was done using the DECH software.[4]

[3] https://www.cfht.hawaii.edu/Instruments/Spectroscopy/Espadons/
[4] http://www.gazinur.com/Spectra-Processing.html

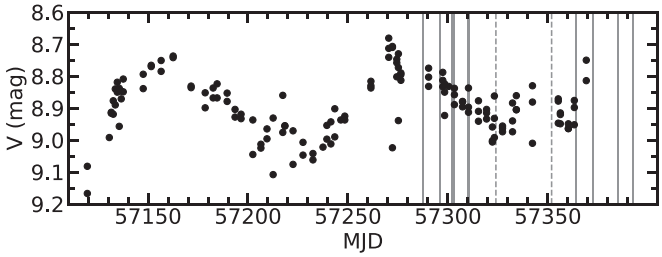

Figure 1. The ASAS-SN light curve of IRAS 22272+5435 near the time of the 2015 September–2016 January spectroscopic observations. The times corresponding to the spectra presented in this study are marked by vertical solid lines, and for other available spectra (October 28 and November 25), dashed lines are used.

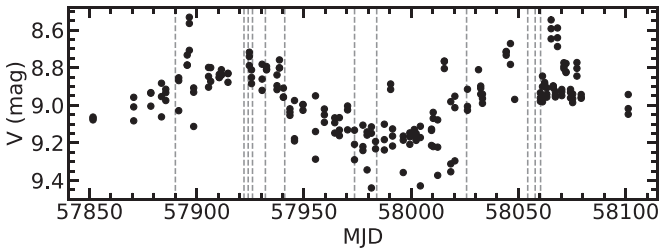

Figure 2. Same as Figure 1 but for the 2017 May–November spectroscopic observations.

We use All-Sky Automated Survey for Supernova (ASAS-SN; Shappee et al. 2014; Kochanek et al. 2017) data to assign pulsation phases to the presented spectra (Figure 1). The phases are estimated by using the minimum magnitude at MJD ≈ 57,271 as the pulsation phase maximum and the period of 132 days and defining that the maximum light corresponds to phase = 0.5. Additionally, we present a light curve[5] for the VUES 2017 May–October spectra, as well as other ESPaDOnS spectra of IRAS 22272+5435 available at the CFHT Science Archive (Figure 2). These are not presented in this study, but some of them are discussed. We estimate the possible range of the pulsation phase by roughly assuming a magnitude minimum at MJD ≈ 57,910 and maximum at MJD ≈ 57,990, with the former serving as the lower and the latter as the upper boundary for the pulsation phase. The chosen dates for the pulsation phase extrema are in line with photometric observations by Hrivnak et al. (2022).

3. Analysis

3.1. September–October Spectra

By inspecting the September–October spectra, a peculiarity is evident: numerous weak emissions on September 22 and 30. Starting from the bluest wavelengths, the first emissions we observe in between plentiful photospheric metal absorption lines are located at around 5100–5150 Å. From 5430 Å onward, similar features are seen. The emissions are most prominent on September 22, typically reaching an intensity of no more than 5% above the continuum level. Afterward, they gradually disappear or turn into absorptions. Especially pronounced emissions, reaching around 10% above the continuum, are seen at 5585.5, 5612.5, and 5635.5 Å. After the latter wavelength emissions are absent until they start to appear at approximately 6060 Å. Here the emissions are

[5] Only "bc" camera data are used because "bd" camera magnitudes are systematically lower and fewer in number.

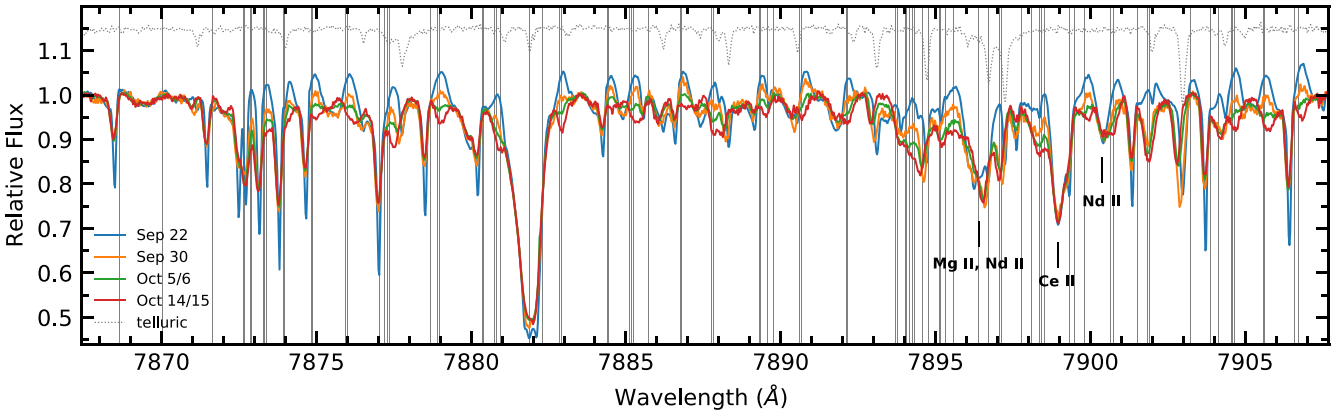

Figure 3. Variation in the September–October spectra of IRAS 22272+5435 in the wavelength region from 7868 to 7907 Å. September 22, September 30, October 5/6, and October 14/15 spectra are shown with blue, orange, green, and red lines, respectively. The gray dotted line is the telluric spectrum. The strongest photospheric absorptions are identified; the one at 7881.9 Å is due to Y II. Gray vertical lines show the positions of the strongest ($\log gf > -4$) CN Red (2, 0) system transitions. The three lines at 7868.7, 7870.0, and 7871.6 Å that appear to show no variation are of $\Delta J = 2$ transitions. The lines shown longward that do exhibit emission and significant variability belong to the R and Q branches ($\Delta J = +1$ and 0).

located rather sparsely, but toward longer wavelengths they tend to be more prominent and seen in greater numbers. Regions with relatively more pronounced emissions are 7090–7170, 7350–7390, and 7455–7594 Å, and very intense emission regions reaching 8%–10% above the continuum or sometimes slightly higher are 7950–8020, 8065–8640, 9115–9225, 9240–9300, 9670–10025, and 10075–10425 Å.

In addition to the wealth of mainly neutron-capture element absorption lines in the spectrum of IRAS 22272+5435, the emissions in the September 22 and 30 spectra make continuum normalization particularly challenging. However, the analyzed spectra belonging to the same pulsation cycle and being closely spaced in time relative to the pulsation period provide generally low temporal variation of metallic absorptions. Therefore, comparison of the analyzed spectra allows us to reliably select normalization points for the continuum level not to be affected by emissions and their variability, at least in the spectral regions where emissions are not too extreme.

Due to emissions being mostly weak and their variation not very pronounced in the spectral regions with the most confidently placed continuum, we summed the October 6 and 7, as well as the October 14 and 15, spectra to increase the S/N. We note that small changes in the emission-related features are also seen between both the October 6 and 7 spectra and the October 14 and 15 spectra. In the former case, the variation follows the general trend of decreasing intensity, but in the latter case, the reverse is often true; absorption is stronger on October 14 than October 15.

3.1.1. CN Lines

By using a CN molecule line list and data from Kurucz calculations based on the observed energy levels that we extracted from VALD (Piskunov et al. 1995; Kupka et al. 1999), we are able to identify virtually all variable emissions longward of 6191 Å with the strongest CN Red system lines. A large part of the emissions seen in the ESPaDOnS spectrum in wavelengths longer than the VUES reach of 9096 Å are also caused by CN Red system transitions. Specifically, we observe $\Delta v = 1$ emissions up to the (3, 2) band, $\Delta v = 2$ up to (5, 3), $\Delta v = 3$ up to (7, 4), and $\Delta v = 4$ up to (7, 3). Emissions are identified to arise from transitions with rotational quantum numbers as high as $J \approx 70$ for the (1, 0) and (2, 1) lines. In the case of other vibrational bands, this number is no lower than 30.

The variability of the (2, 0) lines is shown in Figure 3. A correlation between the positions of the variable emissions and strongest CN lines can be seen. Some of the transitions that cause emissions also give rise to narrow and blueshifted absorptions that are known to originate in the AGB ejecta (Bakker et al. 1997). While the narrow absorptions can be seen in the $J'' \lessapprox 6$ transitions of the (1, 0), (2, 0), (3, 0), and (4, 0) bands, significant emission components are detected in only a few of these low J'' lines that belong to the (1, 0) and (2, 0) bands.

Mostly, individual CN emission features do not belong to a single transition; rather, they are a blend of multiple CN lines. The region with some of the most extreme variability is shown in Figure 4, illustrating well that it is hard to find emissions that we can confidently identify as being caused by only a single CN transition and that are not blended by strong or multiple weak neighboring molecular features or photospheric and telluric absorptions. The few lines for which we are more or less confident that they are not significantly blended and come from a single CN transition are shown in Figure 5. It can be seen that on September 22, the emission peak is at around +3.2 km s^{-1} with respect to systemic velocity, for which we adopt the value of −40.8 km s^{-1} following Začs et al. (2016). Inspection of all CN emissions seen in the spectrum confirms this average value. The FWHM of the emission is, on average, 13 km s^{-1}. Additionally, it appears that there is some weak absorption at around −12 km s^{-1}. Note that this is a larger blueshift than that of the narrow AGB ejecta absorptions, which we measure to be positioned approximately at −7.5 km s^{-1}. On September 30, the emissions are located at about the same position except for the (4, 2) lines, as well as one of the (4, 1) transitions, which seem to have a peak radial velocity closer to the systemic velocity or even slightly blueshifted. On October 14/15, the blueshifted emission component has diminished or transformed into absorption, and hints of very weak emission components that are blueshifted by around 7 km s^{-1} are visible. By inspecting other variable emission lines in the spectra, we observe the tendency for the (2, 0), (3, 0), and (3, 1) features on October 14/15 to be in absorption; however, for at least some of the (4, 1), (4, 2), (5, 2), and (6, 3) lines,

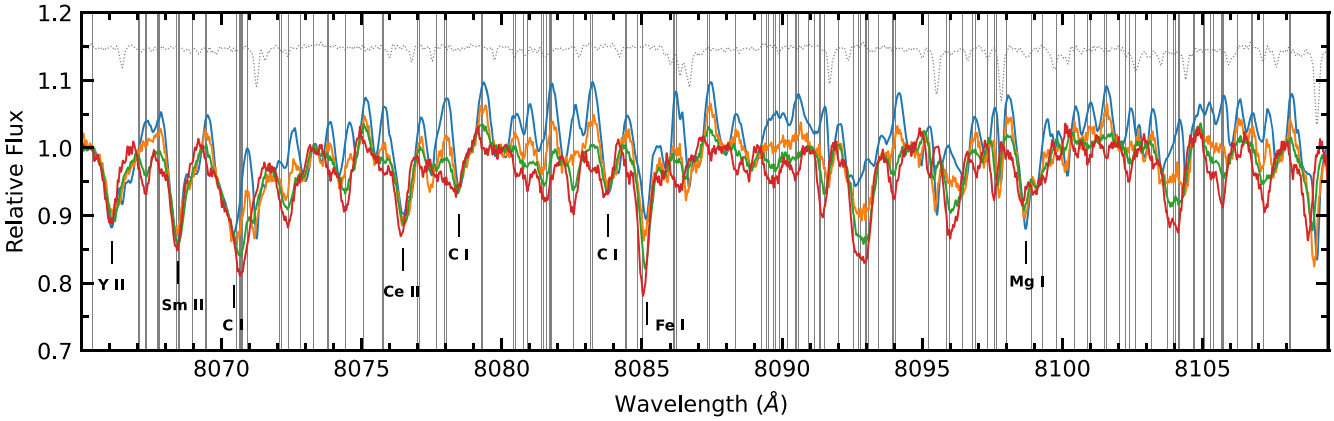

Figure 4. Same as Figure 3 but for the wavelength region from 8065 to 8109 Å. The positions of the strongest ($\log gf > -3$) CN Red (3, 1) and (2, 0) system transitions are shown.

absorption is not as pronounced or even not seen, with only a very weak emission being present.

3.1.2. C_2 Lines

We identify the emissions at 6060–6191 Å and shortward of 5635.5 Å to be caused by C_2 Swan system transitions by using the Kurucz C_2 line list based on observed energy levels. The former belong to the (0, 2) and (3, 1) vibrational bands. The strong emission at 5635.5 Å is caused by the (0, 1) bandhead. This is illustrated in Figure 6, where it can be seen that the variability associated with molecular emissions is partially masked by metallic absorptions. A very similar picture is seen for the (1, 2) bandhead and corresponding lines. Weaker emissions are seen in the (2, 3) lines and bandhead. The few emissions in the 5100–5150 Å region appear to be mainly caused by (0, 0) lines; however, for these and other $\Delta v = 0$ and -1 lines, the bandheads are in absorption. High blending of photospheric absorptions and difficulties in finding any reliable emission that could potentially be caused by a single transition forbid us from a detailed analysis of the profiles of variable emissions. However, it seems that on September 22, the positions of emissions and their widths roughly agree with the values measured for CN lines.

By using the Chen et al. (2015) line positions, we identify emission components in some C_2 Phillips band lines in all September–October spectra, along with the narrow AGB ejecta absorption. In addition to the emissions mainly in the (1, 0) lines that were already reported by Schmidt et al. (2013), we observe them in some (2, 0) and possibly (3, 0) lines as well. We see both the redshifted emission and the narrow absorption in nearly all (1, 0) lines. The emission components appear to have the same velocity and width as the CN emissions. However, we have no conclusive evidence for any variation of these features to be intrinsic to the C_2 Phillips system. The most noticeable variation in the (2, 0) emissions is probably due to blends with the variable CN lines. We observe weak, narrow AGB ejecta absorptions that have not been reported previously in the (3, 1), (4, 1), and (5, 1) lines. In the latter case, they are extremely weak and barely noticeable in our highest R and S/N spectrum from September 22.

3.2. December–January Spectra

Inspection of the December–January spectra also reveals emission in molecular lines, but this time it appears that we observe their emergence rather than decline. On December 7, absorptions are seen in the CN Red and C_2 Swan lines, and on December 16, a few very weak emissions are already visible. On December 28 and January 5, the emissions are almost identical to the ones observed on September 22 in terms of the specific transitions visible and their strengths. The evolution of molecular features in the December–January spectra is presented in Figure 7, and a more detailed look at a few CN Red lines is given in Figure 8. Molecular absorptions on December 5 are redshifted by 2–3 km s^{-1} with respect to the systemic velocity. On December 16, weak emission that is blueshifted by around 5 km s^{-1} is visible. Emissions on December 28 and January 5 are nearly identical, with the exception that the latter peaks at systemic velocity, while the former appears to be blueshifted by approximately 1 km s^{-1}. The FWHMs of these emission lines are about the same as on September 22. As for the C_2 Phillips lines, the situation is similar to that in the September–October spectra; mission components are redshifted by 2–3 km s^{-1} with respect to the systemic velocity and have a similar intensity and width as in the previous spectra. Again, comparison among the December–January and with the September–October spectra gives no definitive evidence for intrinsic variability. If C_2 Phillips emissions do vary on short timescales, their changes are far less pronounced than those in the CN Red and C_2 Swan lines.

3.3. Other Spectra

The two more VUES observations after the presented September–October and before the December–January spectra show absorptions in molecular lines, as expected from the star being in the pulsation phase closer to light minimum (Začs et al. 2016). On October 28, the CN Red and C_2 Swan absorptions are stronger than the ones seen on October 14/15 but weaker than on December 7. On November 25, the molecular absorptions are stronger than on December 7. Analysis of the few least blended CN lines suggests that on October 28, these absorptions are redshifted by some 3 km s^{-1}, and on November 25, they are blueshifted by around 1 km s^{-1} with respect to the systemic velocity.

Inspection of the rest of the available spectra of IRAS 22272+5435 from 2016 and 2017 reveals CN Red and C_2 Swan emissions to be present in some of them as well. We notice weak CN Red and C_2 Swan emissions in the 2016 October 12 spectrum. The CN Red lines appear to be comparable in

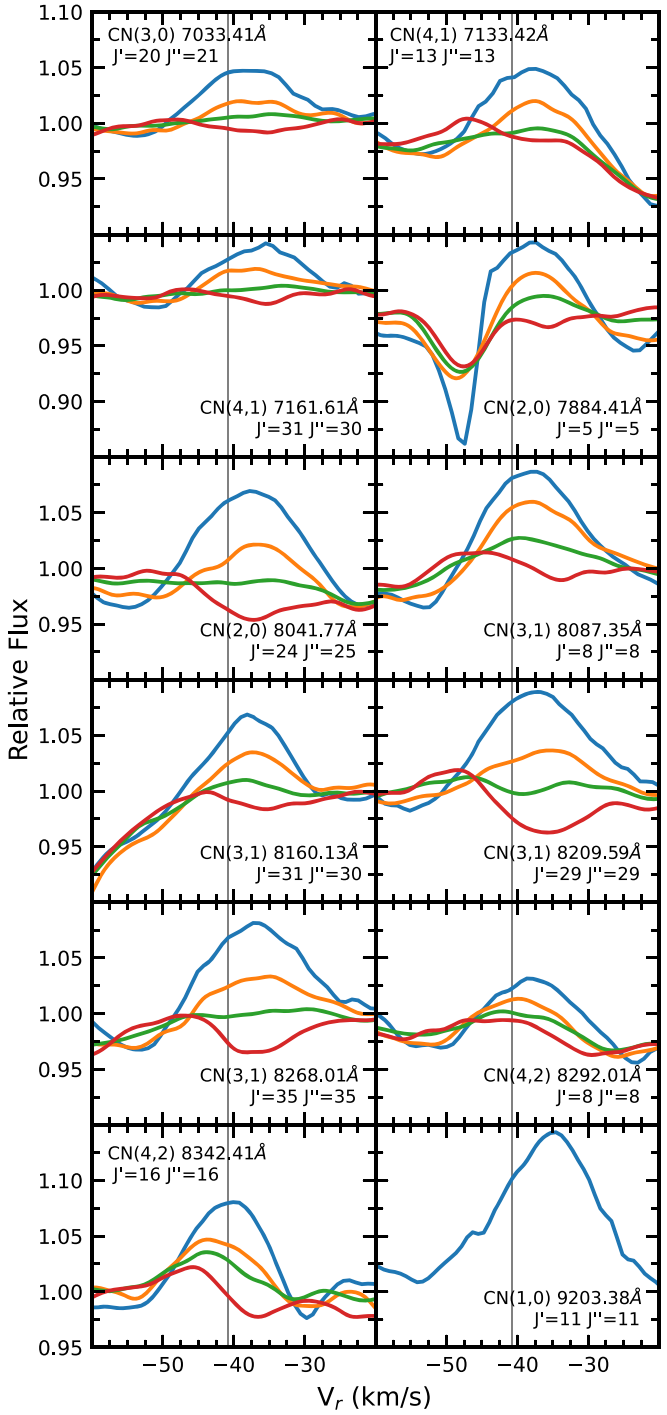

Figure 5. Variability of some of the less blended CN Red system molecular emissions in heliocentric radial velocity scale in the September–October spectra. The colors correspond to the same spectra as in Figure 3. Gray vertical lines show the systemic velocity of -40.8 km s^{-1}. Vibrational bands, wavelengths, and lower (J'') and upper (J') level rotation quantum numbers of the transitions are shown. Noise in the VUES spectra is smoothed out using a Gaussian with an FWHM corresponding to $R = 90{,}000$. The AGB ejecta absorption component of the 7884.41 Å line appears to exhibit minor variability as well; however, we believe that it is caused by the variation of the other (variable emission) component of the same line.

strength and velocity with the 2015 December 16 molecular features and the very weak blueshifted emission components in the September 14/15 spectrum. Although there are ASAS-SN data available for this epoch, the magnitudes are rather chaotic, and no pulsation minimum and maximum can be defined. Extrapolating the light curve shown in Figure 2 backward results in 2016 October 12 corresponding to a pulsation phase of 0.60–0.71. However, in the Hrivnak et al. (2022) observations, the prior light maximum is visible, and it suggests a pulsation phase of approximately 0.77 for October 12. Emissions are also seen in the 2017 January 11 spectrum, and they are similar to the 2015 September 30 molecular features. Unfortunately, there are no magnitude measurements available near this date except for a single observation 9 days prior by Hrivnak et al. (2022) showing high brightness and therefore indicating a pulsation phase close to maximum. Extrapolating the ASAS-SN light curve backward would suggest that 2017 January 11 corresponds to a pulsation phase of 0.29–0.40. There appear to be emissions similar to the ones observed on 2015 September 30 in the 2017 June 17 (MJD = 57,922) spectrum. Although we have four more spectra until 2017 July 6 at our disposal, a detailed analysis of the evolution of the molecular emissions is not possible due to the S/N being low—approximately 50 and lower. We can only state that during this time, the emissions transform into absorptions. The June 17 spectrum corresponds to a pulsation phase of 0.49–0.58, and July 6 is 0.63–0.74. The 2017 October 31 (MJD = 58,058) VUES spectrum and the October 28 and November 3 ESPaDOnS spectra, which correspond to pulsation phases of 0.49–0.64, show molecular lines to be in absorption. The molecular spectra are also described by absorptions for 2017 May 16, August 8 (ESPaDOnS spectrum), August 18, and September 29.

We used the ESPaDOnS 2015 September 22 and 2017 October 28/November 3 spectra to compare the C_2 Phillips system (1, 0) lines, which are not as blended by CN Red transitions as the C_2 Phillips (2, 0) lines. While prominent emissions are seen in the 2015 spectrum, they are absent in the 2017 spectra.

4. Discussion

We have observed broad and slightly redshifted or blueshifted CN Red, C_2 Swan, and C_2 Phillips system molecular emissions in multiple spectra of IRAS 22272+5435 from 2015 to 2017. The spectra we analyze show emissions that generally are no stronger than around 10% above the continuum level and shifted with respect to the systemic velocity by a few kilometers per second. The CN Red lines are variable; it takes around 2–3 weeks for emissions from the maximum intensity to turn into absorptions. The same time is necessary for the emissions to reach the maximum observed intensity since their appearance. The C_2 Swan emissions also exhibit such variability. At the same time, we find no conclusive evidence for such short-term variation in C_2 Phillips lines. There seems to be a correlation of the observed CN Red and C_2 Swan emissions with the pulsation of the star; they are apparent in phases that are closer to light maxima than light minima. Also, Začs et al. (2016) suspected weak CN Red (5, 1) emissions during light maxima phases. However, this correlation does not hold in all cases. In the 2017 October/November spectra, which correspond to pulsation phases near maximum light when emissions would be expected, we observe the molecular features to be in absorption. Additionally, we detect prominent emission in CN Red (1, 0) system lines (Figure 5) in the 2015 September 22 spectrum (shortly after maximum light), but in the 2010 September spectrum that corresponds to light

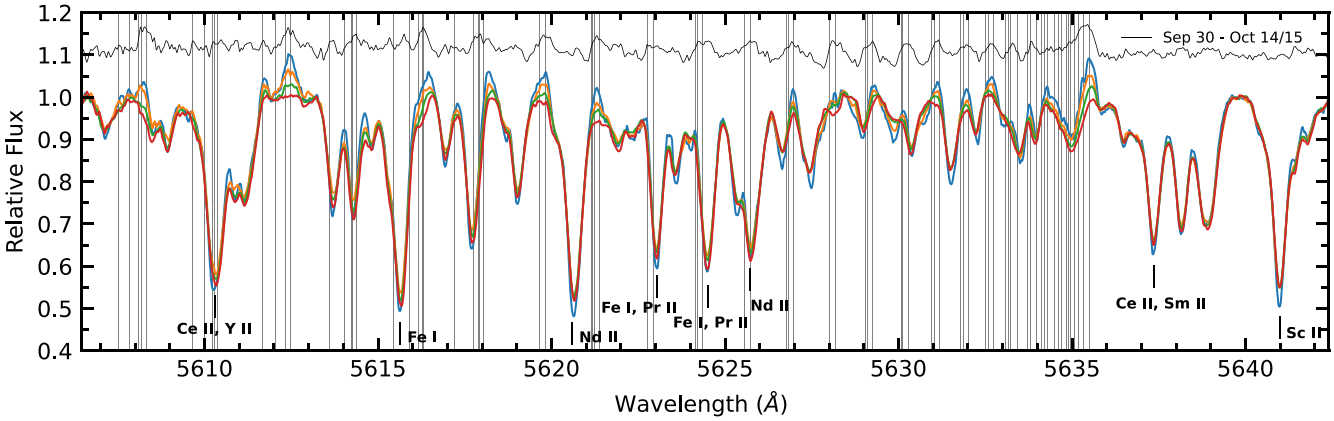

Figure 6. Same as Figure 3 but for the wavelength region from 5607 to 5642 Å. The locations of the strongest ($\log gf > -3$) C_2 Swan (0, 1) system transitions are shown by vertical gray lines. The thin black line depicts the result of the subtraction of October 14/15 from the September 30 spectrum. The VUES spectra are smoothed. Not being affected by the photospheric absorptions contributes to the high level above the continuum for emission at 5612.5 Å.

maximum, Začs & Puķītis (2021) observed them to be in absorption.

This is first time the evolution of CN and C_2 emissions has been traced in post-AGB stars. The proposed mechanisms that cause the optical molecular emission observed in other post-AGB objects do not always agree among different studies. For IRAS 04296+3429, Klochkova et al. (1999) proposed that resonance fluorescence in the circumstellar envelope is responsible for emissions in the C_2 Swan bands. Klochkova et al. (2000b) argued that the same mechanism operates for RAFGL 2688. Klochkova et al. (2000a) suggested that molecular emissions in the optical spectra of IRAS 04296 +3429, RAFGL 2688, IRAS 23304+6147, and IRAS 22223 +4327 are visible due to the high obscuration of the central star that allows for the weak emissions originating in the extended nebula to be seen. Sánchez Contreras et al. (2008) observed C_2 Swan emissions in IRAS 04296+3429 from the compact (unresolved) nuclear region. Balm & Jura (1992) suggested that the most probable CH^+ emission mechanism in RAFGL 915 is radiative excitation followed by rapid fluorescent decay. Bakker et al. (1997) discussed that the line-forming region of CH^+ emissions is not very extended and could be related to shocked regions. According to Hobbs et al. (2004), CH^+ emissions originate primarily within or near the small, dusty torus that obscures the central star.

Also, for the CO $\Delta v = 2$ bands, variation in the emission intensities is observed in post-AGB stars. Hrivnak et al. (1994) explained the observed transformation from emission to absorption of these features in IRAS 22272+5435 by mass ejection from the central star. The molecules are collisionally excited, and emission originates either at the base of a new (post-AGB) wind where the density is high or at the region of interaction between this flow and the outer (AGB) envelope where the shock energy is dissipated. The latter is suggested as the explanation in the case of IRAS 19114+0002 and IRAS 22223+4327, for whom CO emission without any significant variation was observed. Later, Venkata Raman & Anandarao (2008) did not detect any significant CO-band emission in these two stars. Oudmaijer et al. (1995) reported another two post-AGB objects with variable CO emissions: HD 170756 and HD 101584. A scenario in which the emission originates within a few stellar radii of the photosphere is favored, and in the case of HD 170756, the possibility of the emissions being related to episodic mass loss during the pulsation cycle is presented. Mozurkewich et al. (1987) observed variable CO emission/absorption profiles in the RV Tauri–type star R Scuti and attributed them to shocks in the upper atmosphere. Integral field spectroscopy of the post-AGB object IRAS 18276–1431 supports the idea that CO emissions form close to the star (Gledhill et al. 2011).

The fast changes and large widths of the emission and absorption components of the CN Red features that we observe in IRAS 22272+5435, as well as the previous works on CO $\Delta v = 2$ band variability, lead us to conclude that the molecular emissions that we observe originate within a few stellar radii above the photosphere of the star. No detailed modeling of dynamics in such close vicinities of post-AGB objects has been done; however, it has been performed for the extended atmospheres of AGB stars. Although post-AGB stars are more compact and hotter, in the case of the cooler ones, like IRAS 22272+5435 (see Začs & Puķītis 2021), AGB models could be more reliably applied to them. Even a simple modeling of dynamics by introducing a spherically symmetric outflow or infall on a hydrostatic atmosphere structure can produce emission components in CO $\Delta v = 2$ molecular lines similar to those we see in IRAS 22272+5435 for CN Red lines (Nowotny et al. 2010). However, a different molecule is in question, and, additionally for such a simple scenario, intense absorption components are expected, but in our case, they are very weak. If one would assume that outflow/infall in the line of sight happens to be less dense than in other directions, the strength of absorption would be lower. Perhaps the opposite situation is the cause of the molecular absorptions in the 2017 October/November spectra. Large-scale deviations from spherical symmetry caused by convection, as well as outflows and infalls, have been observed in three-dimensional simulations of AGB stars (Freytag & Höfner 2008; Freytag et al. 2017; Liljegren et al. 2018). In the 2015 September 22 and 30 spectra, the redshifted emission along with weak blueshifted absorption resembles a P Cygni–type profile, suggesting that the formation of molecular lines might be related to an outflow. On October 14/15, redshifted absorption and weak blueshifted emission resembles an inverse P Cygni–type profile, therefore hinting at a reverse situation: infall of matter. Additionally, the low velocities that we measure in variable molecular emission/absorption components are consistent with the results of three-dimensional modeling. The fact that C_2 Phillips emissions seem to be not as variable as CN Red and C_2 Swan emissions might

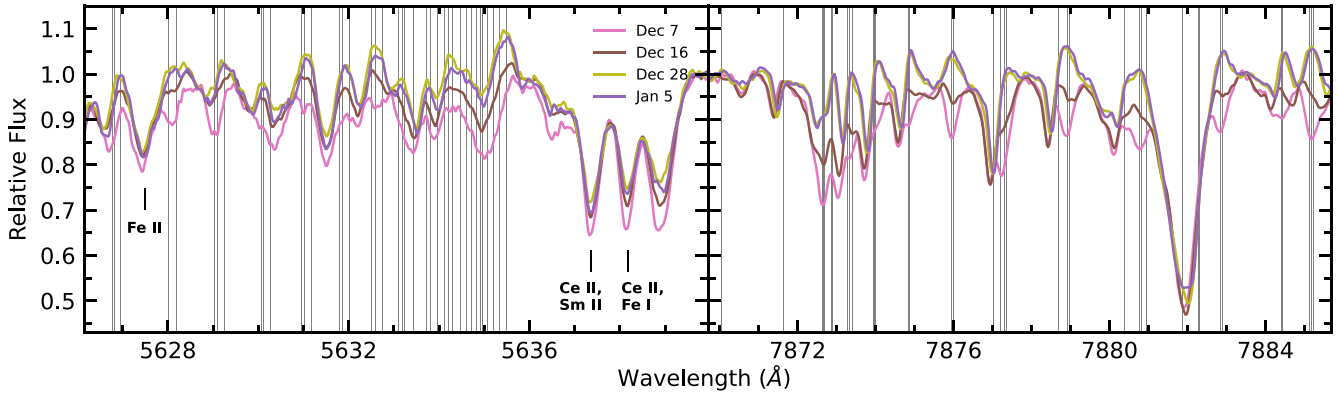

Figure 7. Variation in the December–January spectra of IRAS 22272+5435 in the C_2 Swan (0, 1) (left) and CN Red (2, 0) (right) bandheads. The December 7, December 16, December 28, and January 5 spectra are shown with pink, brown, olive, and violet lines, respectively. The positions of the strongest molecular transitions are marked by gray vertical lines.

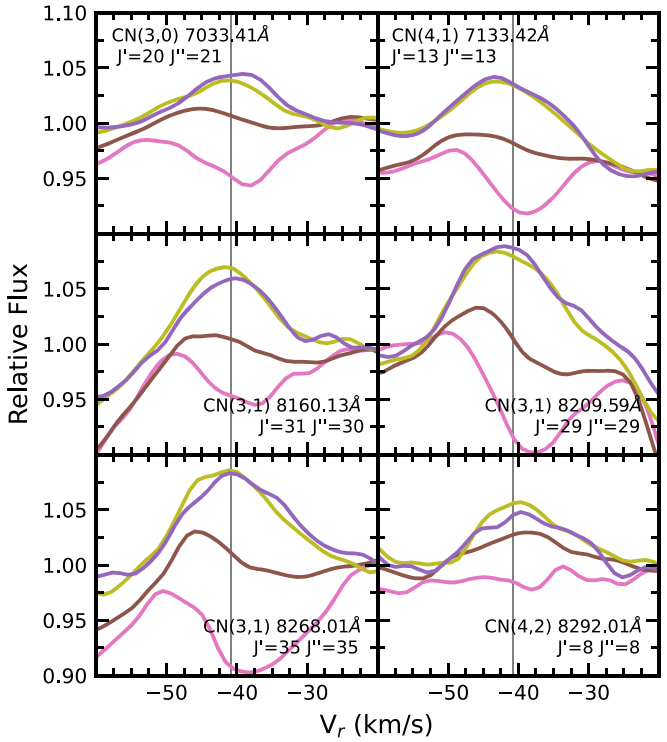

Figure 8. Same as Figure 5 but for a few lines in the December–January spectra. The colors are the same as in Figure 7.

be related to the formation of spectral features at different heights above the photosphere. However, we stress that the above interpretation should in no way be regarded as a complete explanation, since it does not account for the apparent connection of the emissions with the pulsation of the star, and the situation is probably more complex, for example, with shocks playing a role in changes of the upward/downward motions and excitation of molecules. The idea is merely to show that, in principle, the observed molecular features could be formed within a few stellar radii above the photosphere.

K.P. acknowledges support from the project "Strengthening of the Capacity of Doctoral Studies at the University of Latvia within the Framework of the New Doctoral Model," identification No. 8.2.2.0/20/I/006. L.Z. acknowledges funding from the Latvian Council of Science, project "Advanced spectroscopic methods and tools for the study of evolved stars," project No. lzp-flpp-2020/1-0088. This research used the facilities of the Canadian Astronomy Data Centre, operated by the National Research Council of Canada with the support of the Canadian Space Agency. This work has made use of the VALD database, operated at Uppsala University, the Institute of Astronomy RAS in Moscow, and the University of Vienna.

Software: DECH (http://www.gazinur.com/Spectra-Processing.html).

ORCID iDs

Kārlis Puķītis https://orcid.org/0000-0003-2599-6126
Laimons Začs https://orcid.org/0000-0001-9301-3721
Julius Sperauskas https://orcid.org/0000-0003-0931-7744

References

Bakker, E. J., van Dishoeck, E. F., Waters, L. B. F. M., & Schoenmaker, T. 1997, A&A, 323, 469
Balm, S. P., & Jura, M. 1992, A&A, 261, L25
Bollen, D., Kamath, D., Van Winckel, H., et al. 2022, A&A, 666, A40
Chen, W., Kawaguchi, K., Bernath, P. F., & Tang, J. 2015, JChPh, 142, 064317
Donati, J. F., Semel, M., Carter, B. D., Rees, D. E., & Collier Cameron, A. 1997, MNRAS, 291, 658
Freytag, B., & Höfner, S. 2008, A&A, 483, 571
Freytag, B., Liljegren, S., & Höfner, S. 2017, A&A, 600, A137
Gledhill, T. M., Forde, K. P., Lowe, K. T. E., & Smith, M. D. 2011, MNRAS, 411, 1453
Hobbs, L. M., Thorburn, J. A., Oka, T., et al. 2004, ApJ, 615, 947
Hrivnak, B. J., Kwok, S., & Geballe, T. R. 1994, ApJ, 420, 783
Hrivnak, B. J., Lu, W., Bakke, W. C., & Grimm, P. J. 2022, ApJ, 939, 32
Hrivnak, B. J., Lu, W., Sperauskas, J., et al. 2013, ApJ, 766, 116
Jurgenson, C., Fischer, D., McCracken, T., et al. 2016, JAI, 5, 1650003
Klochkova, V. G. 2014, AstBu, 69, 279
Klochkova, V. G., Panchuk, V. E., & Tavolzhanskaya, N. S. 2010, ARep, 54, 234
Klochkova, V. G., Szczerba, R., & Panchuk, V. E. 2000a, AstL, 26, 88
Klochkova, V. G., Szczerba, R., & Panchuk, V. E. 2000b, AstL, 26, 439
Klochkova, V. G., Szczerba, R., Panchuk, V. E., & Volk, K. 1999, A&A, 345, 905
Kochanek, C. S., Shappee, B. J., Stanek, K. Z., et al. 2017, PASP, 129, 104502
Kupka, F., Piskunov, N., Ryabchikova, T. A., Stempels, H. C., & Weiss, W. W. 1999, A&AS, 138, 119
Lèbre, A., Mauron, N., Gillet, D., & Barthès, D. 1996, A&A, 310, 923
Liljegren, S., Höfner, S., Freytag, B., & Bladh, S. 2018, A&A, 619, A47
Mozurkewich, D., Gehrz, R. D., Hinkle, K. H., & Lambert, D. L. 1987, ApJ, 314, 242
Nowotny, W., Höfner, S., & Aringer, B. 2010, A&A, 514, A35
Oudmaijer, R. D., Jones, E. R. M., & Vioque, M. 2022, MNRAS, 516, L61

Oudmaijer, R. D., Waters, L. B. F. M., van der Veen, W. E. C. J., & Geballe, T. R. 1995, A&A, 299, 69
Piskunov, N. E., Kupka, F., Ryabchikova, T. A., Weiss, W. W., & Jeffery, C. S. 1995, A&AS, 112, 525
Sánchez Contreras, C., Sahai, R., Gil de Paz, A., & Goodrich, R. 2008, ApJS, 179, 166
Sarre, P. J., Miles, J. R., & Scarrott, S. M. 1995, Sci, 269, 674
Schmidt, G. D., Cohen, M., & Margon, B. 1980, ApJL, 239, L133
Schmidt, M. R., Začs, L., Pułecka, M., & Szczerba, R. 2013, A&A, 556, A46
Shappee, B. J., Prieto, J. L., Grupe, D., et al. 2014, ApJ, 788, 48
Ueta, T., Meixner, M., Hinz, P. M., et al. 2001, ApJ, 557, 831
Venkata Raman, V., & Anandarao, B. G. 2008, MNRAS, 385, 1076
Začs, L., Musaev, F., Kaminsky, B., et al. 2016, ApJ, 816, 3
Začs, L., & Puķītis, K. 2021, ApJ, 920, 17
Začs, L., & Puķītis, K. 2023, ApJ, submitted
Začs, L., Sperauskas, J., Musaev, F. A., et al. 2009, ApJL, 695, L203